

## ORIGINAL ARTICLE

# Homogeneous dewetting on large-scale microdroplet arrays for solution-processed electronics

Xuying Liu<sup>1,2,6</sup>, Chuan Liu<sup>3,6</sup>, Kenji Sakamoto<sup>2</sup>, Takeshi Yasuda<sup>2</sup>, Pan Xiong<sup>2</sup>, Lijuan Liang<sup>2</sup>, Tengzhou Yang<sup>3</sup>, Masayuki Kanehara<sup>4</sup>, Jun Takeya<sup>2,5</sup> and Takeo Minari<sup>2,5</sup>

Unidirectional dewetting enables the production of large-area thin films with high efficiency at low cost. Herein, we report homogeneous unidirectional dewetting on large-area microdroplet arrays via gravity-induced deformation in droplets combined with alternating lyophilic/lyophobic patterns. This process allows the scaled-up deposition of thin films, including organic semiconductors and transition metal oxides, through the autogenous shrinkage of droplets, which further enables the fabrication of large-area organic thin-film transistor (OTFT) arrays. The resulting field-effect mobility and on/off ratio of the fully printed OTFTs exceeded  $13 \text{ cm}^2 \text{ V}^{-1} \text{ s}^{-1}$  and  $10^8$ , respectively. Therefore, the presented dewetting method is promising to realize the roll-to-roll manufacture of large-area flexible electronics.

*NPG Asia Materials* (2017) 9, e409; doi:10.1038/am.2017.123; published online 28 July 2017

## INTRODUCTION

Dewetting phenomena are widely investigated at present since they provide fundamental understanding of microfluid dynamics<sup>1–8</sup> and solutions for practical applications, including microfluidic devices,<sup>1,2</sup> anti-icing surfaces<sup>5</sup> and protein micropatterns.<sup>8</sup> Particularly, dewetting organic semiconductor inks on a smooth surface enables the deposition of organic semiconductor thin films and electronic devices.<sup>9</sup> In general, the dewetting process spontaneously occurs in a droplet when the following condition is satisfied:  $\gamma_{gl} - \gamma_{ls} - \gamma_{gs} < 0$  ( $\gamma_{gl}$ ,  $\gamma_{ls}$  and  $\gamma_{gs}$  are the gas-liquid, liquid-solid and gas-solid surface tensions, respectively). In most cases, the three-phase contact line of an unconfined droplet continuously recedes without shrinking in a certain direction; as a consequence, such unconfined dewetting commonly yields poorly crystalline thin films or inhomogeneous patterns, subsequently leading to inhibited device performance.<sup>10,11</sup>

Inducing unidirectional dewetting has been identified as one of the most effective approaches to deposit highly aligned crystallized thin films for solution-processed electronics with high efficiency at low cost. Therefore, many efforts have aimed to exploit the direction-controlled dewetting by adjusting the moving directions of the upper or bottom substrates or by modifying the substrate surfaces using special treatments.<sup>12–17</sup> For example, Bao and co-workers developed a series of techniques, including shearing and coating, to deposit aligned crystalline thin films; however, these procedures more or less rely on the nanostructures of the shearing blade or of the modified substrate, which are rarely involved in large-scale

implementation.<sup>14–16</sup> Jiang et al. recently reported that a line-pillar-structured template could be employed to guide 3D dewetting to position crystal stripes, but the preparation and removal of the template would probably complicate device fabrication, which would eventually render the scaled-up process more difficult.<sup>17</sup> Therefore, it is still a challenge to selectively deposit aligned crystalline films without a template.

Here, we report a homogeneous dewetting technique on large-area microdroplet arrays (MDAs) (300 MDs,  $4 \text{ cm} \times 4 \text{ cm}$ ) caused by the gravity-assisted deformation of droplets on a tilted substrate, which enables the formation of aligned crystalline thin films for device applications. It was found that increasing the tilt angle enables the deformation of droplets, thus leading to the homogeneous receding of upper contact lines from top to bottom on the MDAs. Moreover, this method allows the deposition of discrete organic semiconducting thin films for fully printed organic thin-film transistors (OTFTs). In particular, when using a tilt angle of  $90^\circ$ , the obtained films exhibit the optimal surface morphology, which could be understood through theoretical interpretations. Furthermore, the dewetting behavior of water enables the selective deposition of transition metal oxides to modify the semiconductor/electrode interface to lower the contact resistance in OTFTs. The contact resistance was significantly decreased from  $14.9 \text{ k}\Omega \text{ cm}$  to  $3.8 \text{ k}\Omega \text{ cm}$  in the fully printed OTFTs, which results in an increase in the field-effect mobility ( $\mu_{\text{FET}}$ ) from  $9.2 \text{ cm}^2 \text{ V}^{-1} \text{ s}^{-1}$  (before treatment) to  $13.1 \text{ cm}^2 \text{ V}^{-1} \text{ s}^{-1}$  (after treatment). The presented method of using

<sup>1</sup>School of Materials Science and Engineering, Zhengzhou University, Henan, China; <sup>2</sup>Materials Nanoarchitectonics (MANA), National Institute for Materials Science (NIMS), Ibaraki, Japan; <sup>3</sup>State Key Laboratory of Optoelectronic Materials and Technologies, Guangdong Province Key Laboratory of Display Material and Technology and School of Electronics and Information Technology, Sun Yat-sen University, Guangzhou, China; <sup>4</sup>C-Ink. Co., Ltd., Okayama, Japan and <sup>5</sup>The University of Tokyo, Chiba, Japan

<sup>6</sup>These authors contributed equally to this work.

Correspondence: Dr T Minari, National Institute for Materials Science (NIMS), 1-1 Namiki, Tsukuba, Ibaraki 305-0044, Japan.

E-mail: MINARI.Takeo@nims.go.jp

Received 11 January 2017; revised 7 April 2017; accepted 2 May 2017

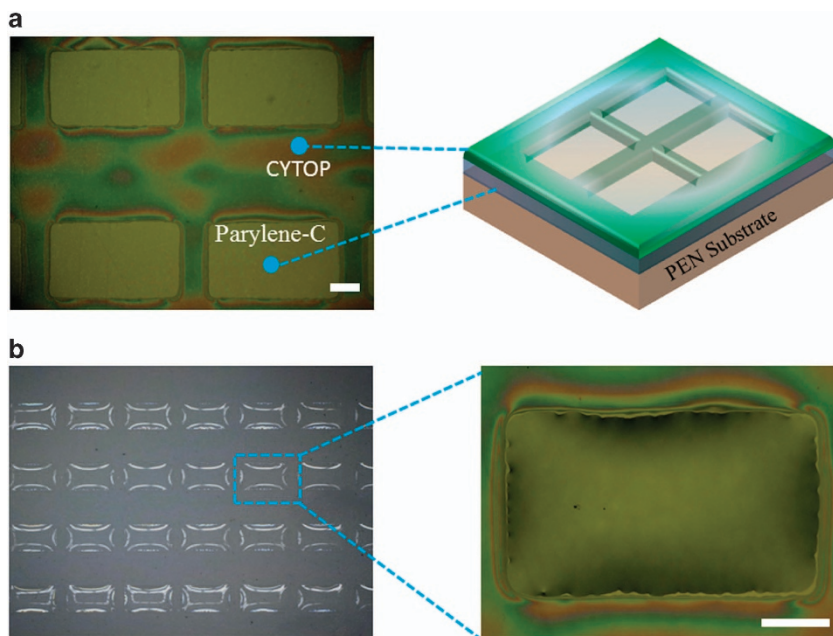


**Figure 1** (a) Photograph and illustration of a Cytop guide layer on a Parylene-C surface. (b) Photographs of an MDA and a microdroplet in the bank with a size of  $500\ \mu\text{m} \times 1000\ \mu\text{m}$ .

homogeneous unidirectional dewetting to selectively fabricate aligned crystalline thin films and doping layers does not need any template and is totally compatible with conventional photolithography, which is widely used in the TFT industry.

## MATERIALS AND METHODS

### Materials

C8-BTBT was received from Nippon Kayaku Co., poly(ethylene 2,6-naphthalate) (PEN) substrates were purchased from Teijin Dupong Film Co., Ltd., and Au nanoparticle ink is available from Colloidal Ink Co., Ltd. All materials were directly used without any modification.

### Fabrication of microdroplet arrays and unidirectional dewetting process

The detachable substrates were prepared via a screen-printing technique as reported in our previous work. The thickness of the screen-printed Cytop guide layer was 500 nm. To adjust the tilt angle, the substrate was fixed on a rotatable stage. Then, the camera lens of the microscope (Keyence Co., Ltd., VHX-2000) was rotated to be vertical to the substrate surface to record the dewetting dynamics. Liquid droplets were simply deposited by a drop-casting method (as shown in Supplementary Movie I), which allowed the micro-scale droplet to be precisely deposited in the bank in a single step. At the initial moment, at the critical inclination angle, the conditions were optimized to satisfy equation (1). As a result, it could be observed that the dewetting process occurred from the top edge to the bottom edge along the inclination plane. Aqueous dopant inks were prepared according to the method described in the Supplementary Information. The microdroplet arrays were formed by the same injection process described above. The volume remaining in the bank was ca.  $0.1\ \mu\text{l}$ , according to the bank size. After the injection was finished, the substrate was laid horizontally for 20 min, which allowed the dewetting and drying of aqueous TMO microdroplets on the AuNP electrodes.

### Fabrication of discrete OTFT arrays

An as-received PEN film (A4 size) was first cut into small pieces ( $4\ \text{cm} \times 4\ \text{cm}$ ) and then treated in a homemade chemical vacuum evaporation system to deposit an 800-nm-thick Parylene-C (KISCO, dix-c) layer as the modification layer. The modified substrates were transferred into a vacuum UV system (172 nm wavelength, Ushio Inc.) and selectively exposed (15–25 seconds)

through a photomask to form patterns, onto which the Au nanoparticle ink could easily adhere to fabricate hydrophilic source and drain electrodes by the coating bar. The printed Au bottom electrodes can be directly used without any annealing or sintering processes. Screen-printing was utilized to construct the guide layer using the original Cytop solution (Asahi Glass Co., Ltd.) through a screening mask, which produced bank arrays with depths of 500 nm in the substrate. Drop-casting a C8-BTBT solution (0.4 wt% in anisole) into the banks and keeping the substrate perpendicular ( $90^\circ$  inclination angle) guarantee the formation of a thin semiconductor film. Then, the guide layer can be removed by washing the substrate using Cytop solvent 180, which was dried at room temperature for 2 hours or by a 20-min annealing process at  $40^\circ\text{C}$ . The dielectric bilayer, with a capacitance of  $2.8\ \text{nF cm}^{-2}$ , includes a 250-nm Cytop and 600-nm Parylene-C; the former was formed by spin-coating, while the latter was deposited by a CVD process. After that, patterning using the VUV method was used again to form top gate electrodes.

## RESULTS AND DISCUSSION

A 125- $\mu\text{m}$ -thick poly(ethylene 2,6-naphthalate) (PEN) sheet with a 2- $\mu\text{m}$  Parylene-C planarity layer was used as a flexible substrate. The banks were formed on the planarity layer by forming a detachable guide layer of 500-nm-thick Cytop using screen-printing (Figure 1a and Supplementary Figure S1).<sup>18,19</sup> As reported,<sup>20</sup> Parylene-C has a good affinity with common organic liquids, while Cytop as a fully fluorinated polymer exhibits highly lyophobic features.<sup>21,22</sup> In this case, when liquid droplets, such as anisole, were placed onto the substrate by drop-casting, they self-assembled into the Parylene-C regions without any external force, as shown in Supplementary Movie I and Figure 1b. This process mainly relies on the difference between the surface free energy of the Cytop surface guide layer and the Parylene-C regions<sup>20</sup> and can be realized even in a high-resolution pattern with various micro-scale pre-patterns (Supplementary Figure S1). Furthermore, it is worth noting that this method is feasible for a wide variety of common liquids (such as water, ethanol, toluene, anisole, dichlorobenzene and N,N-dimethylformamide). Compared with other fabrication methods for MDAs,<sup>23–25</sup> the method described here is easy to handle and can be conveniently scaled up (see Methods Section); it can be generally used in a wide range of

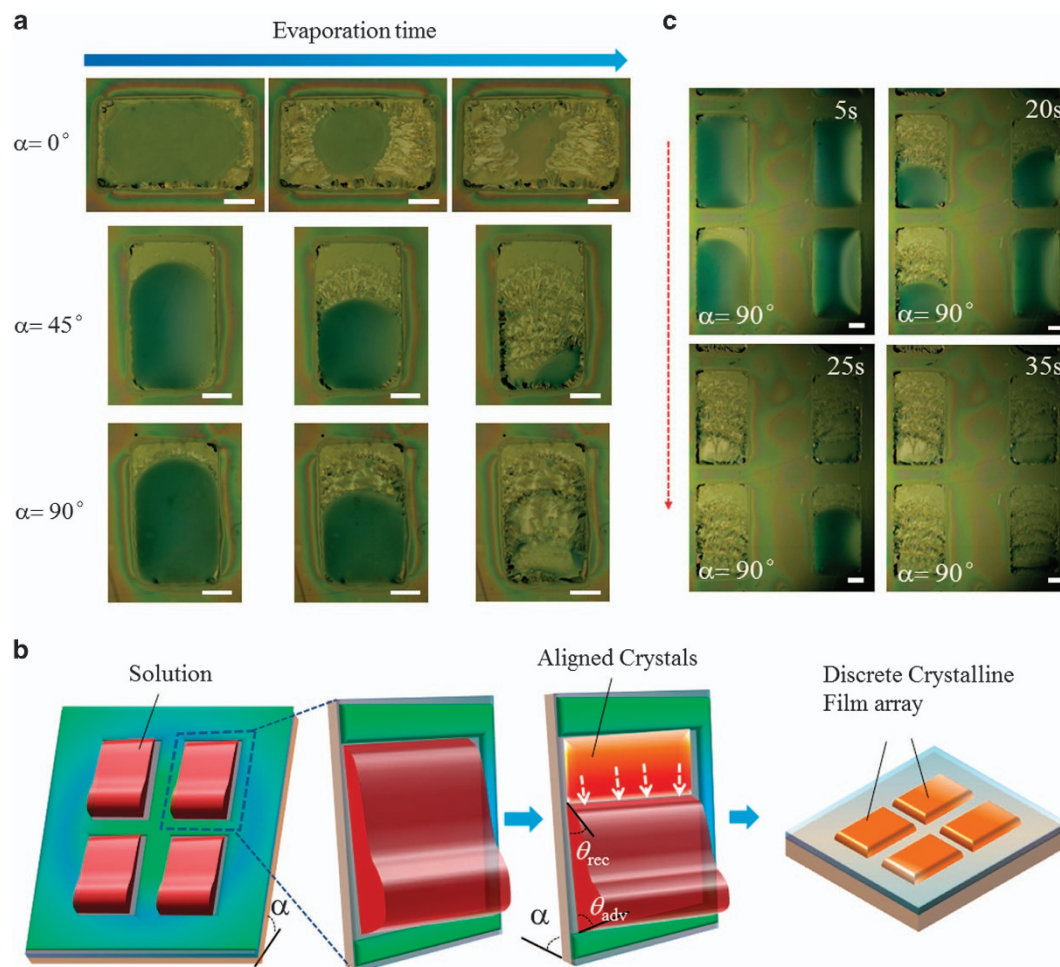


**Figure 2** (a) Real-time observation of the microdroplet dynamics on oblique surfaces with different tilt angles and the surface morphology of the deposited thin films. (b) Homogeneous unidirectional dewetting on 4 microdroplets (selected from 270 microdroplets in an array). The red arrow represents the dewetting direction. (c) Schematic illustration of the dynamic course of the microdroplets in the substrate with a tilt angle of  $90^\circ$ . The white scale bars represent  $200\ \mu\text{m}$ .

solution processes, such as the deposition of thin films and nanoparticle arrays or parallelization assays for culturing cells.

To demonstrate practical applications of the constructed organic MDAs, we fabricated large-area isolated thin film arrays based on the induced unidirectional dewetting. As shown in Figure 2a, the substrate was held horizontally (tilt angle,  $\alpha = 0^\circ$ ), wherein the droplets of anisole had an axisymmetric shape and began to dewet toward their geometric centers, thus yielding radially grown crystalline films. When the substrate was inclined at  $\alpha = 45^\circ$ , the upper contact line of the microdroplet was observed to recede along the oblique plane, while the bottom contact line stayed pinned. This phenomenon originated from the nonaxisymmetric shape of the droplets, which is commonly caused by gravity;<sup>26–28</sup> the nonaxisymmetry in the droplets could render upper regions thinner and bottom regions thicker.<sup>29–32</sup> Subsequently, thin films were smoothly formed following the induced unidirectional dewetting. When the inclination angle  $\alpha$  was increased to  $90^\circ$ , the receding motion of the contact lines accelerated and yielded much more uniform thin films (Figure 2c); hence, the morphology of the crystalline film can be easily controlled by altering the inclination angle that modifies the receding speed of the three-phase contact line.

This unidirectional dewetting process was not observed when using a square-shaped pattern (Supplementary Figure S2), where the

gravity-induced deformation was rather weak. In a longer pattern (the width/length ratio is approximately 1/4), the coffee-stain effect became dominant due to the competitive crystallization between contact line regions and lateral regions (Supplementary Figure S3). Lateral dewetting was observed when the substrate was rotated by  $90^\circ$ , which produced crystals at both the upper and bottom contact lines (Supplementary Figure S4). These results indicate that the droplet deformation induced by gravity is rather important, as it can drag the three-phase contact line to unidirectionally recede.

Further investigation from a theoretical aspect was undertaken to understand the induced unidirectional dewetting that occurred when the inclination angle exceeded the critical tilt angle of  $\alpha_c$  (as indicated in Figure 2b). Presumably, the shapes of all microdroplets can be approximately regarded to be parallel-sided (with a width of  $\omega$ ). According to the model given by Furmidge,<sup>33</sup>  $\alpha_c$  can be defined by the following equation:

$$\sin \alpha_c = \frac{\kappa \omega \gamma_{gl}}{\rho g V} (\cos \theta_{rec} - \cos \theta_{adv}) \quad (1)$$

where  $\rho$  is the liquid density,  $g$  is the acceleration of gravity,  $\gamma_{gl}$  is the liquid/solid surface tension,  $V$  is the volume of the liquid droplet (determined by the bank volumes) and the retention-force factor  $\kappa$  is equal to 2 according to the initial droplet shape.<sup>32</sup> This equation

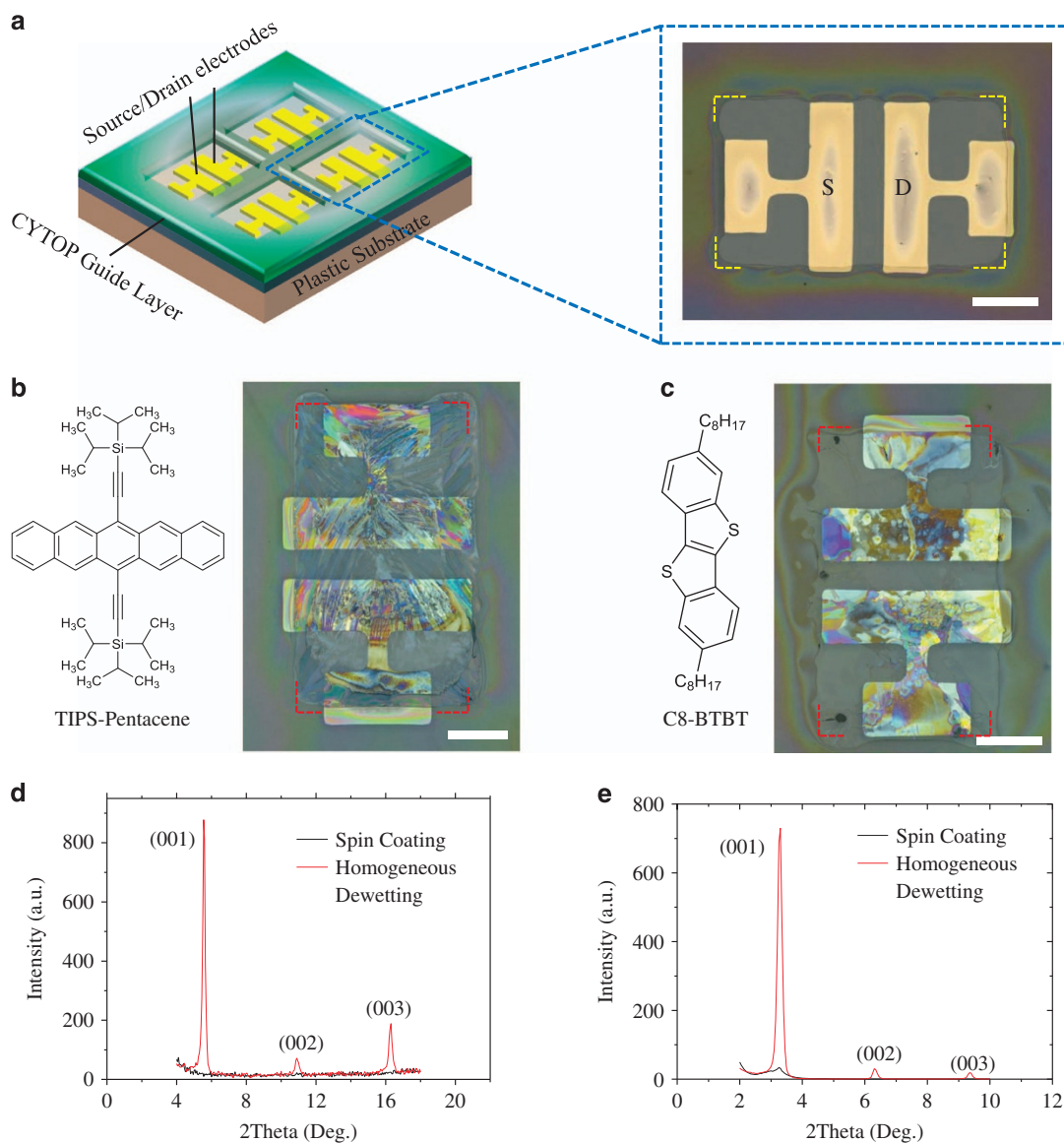


**Figure 3** (a) Illustration and photograph of a Cytop guide layer and source/drain electrodes. (b, c) Molecular structures and deposited crystalline films of TIPS-pentacene and C8-BTBT, respectively. The scale bars are 200  $\mu\text{m}$ . (d, e) XRD patterns of the TIPS-pentacene and C8-BTBT thin films fabricated by spin-coating and homogeneous dewetting, respectively. The inset in e shows the signals for the (002) and (003) peaks.

suggests that  $\alpha_c$  is proportional to the cosine difference of the receding and advancing contact angles, namely,  $\theta_{rec}$  and  $\theta_{adv}$ .

As for organic liquids, such as anisole, the contact angle is quite low, and thus the liquid film on the triple-phase contact line will be rather thin, and  $\theta_{rec}$  will be close to  $0^\circ$ . At the bottom side, the droplet is supported by a Cytop wall, which pins the advancing contact line, thereby yielding a high  $\theta_{adv}$  around  $90^\circ$  at the initial stage. Therefore,  $\alpha_c$  can be approximately estimated by the surface tension and the density of the applied organic liquids. A small  $\alpha_c$  can result from a low surface tension and a high liquid density. According to our observation in commonly used organic liquids, dichlorobenzene has a smaller  $\alpha_c$  than other solvents, including dodecane, xylene, chlorobenzene and anisole, due to it having the highest density among the selected liquids (Supplementary Figure S5), which agrees with the theoretical interpretation. We applied this process into a large-area MDA, on which 270 microdroplets were integrated. It was also observed that the dewetting of an anisole-coated MDA could be

controlled by increasing the tilt angles, as shown in Supplementary Movie II and Figure 2c. When the inclination angle  $\alpha_c$  is larger than the related critical values, the droplets homogeneously exhibited unidirectional dewetting behavior on the large-area array.

Homogeneous unidirectional dewetting was applied to the fabrication of thin active layers for solution-processed OTFT devices. Figure 3a exhibits the source and drain electrodes of gold nanoparticles (AuNPs) pre-deposited with the Cytop banks, and the method was given in our previous reports.<sup>18</sup> When a solution of 6,13-bis(triisopropyl-silylethynyl) pentacene (TIPS-pentacene) in chlorobenzene was applied, long crystalline domains can be observed following the dewetting of chlorobenzene (Figure 3b). Likewise, the droplet of dioctylbenzothienobenzothiophene (C8-BTBT) in anisole during dewetting gave rise to thin crystalline films with large domain sizes of several hundred microns, which completely covered the channel regions (Figure 3c). Such well-aligned crystalline films and fibers (e.g., tetrafluorotetracyanoquinodimethane) showed the same

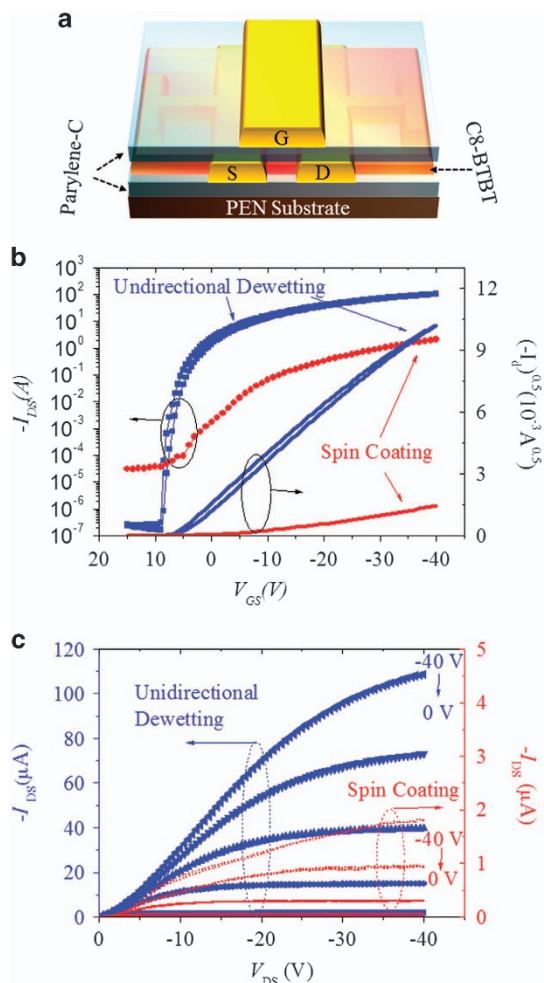


**Figure 4** (a) Device configuration. (b) and (c) Device performance, where the transfer and output characteristics are displayed, respectively. The transistors measured here had the same TFT channel length of 100  $\mu\text{m}$  and the same width of 500  $\mu\text{m}$ , where the active layers of C8-BTBT were fabricated by the unidirectional dewetting method or the spin-coating method, respectively. The applied drain voltages were  $-40\text{ V}$  in **b**. The gate voltage steps were 10 V in **c**.

growth direction as that of unidirectional dewetting, which can be clearly identified through optical microscope observations, as shown in Supplementary Figures S6 and S7, respectively.

The X-ray diffraction patterns in Figure 3d and e reveal that these thin films had a higher degree of crystallinity than those fabricated by spin-coating methods. Very sharp peaks appeared at low angle regions corresponding to the (001), (002) and (003) planes, respectively, which can be comparable with those obtained in their single crystals.<sup>34</sup> In comparison, the related peaks have much lower intensity and broader shape than those of the spin-coated films. Quantitative investigation of the crystallization of C8-BTBT films was performed by analyzing the full width at half maximum (FWHM) of the (001) signals (Supplementary Figure S8). The FWHM values of the films fabricated by spin-coating and by unidirectional wetting were detected to be  $0.50^\circ$  and  $0.20^\circ$ , respectively. Hence, the crystallites in the former case are expected to have much larger domains,<sup>35</sup> which is consistent with the observation in Figure 3 and Supplementary Figure S6. The increased peak intensity, the decreased FWHM, and the higher order of diffraction peaks observed in the film firmly support an increased

order of crystallinity associated with aligned crystallites caused by unidirectional dewetting.

The quality of the deposited thin film arrays can also be evaluated by measuring the charge carrier transport in fully printed bottom contact/top gate OTFTs (shown in Figure 4a). Both TIPS-pentacene and C8-BTBT exhibited typical hole charge transport properties. The values of  $\mu_{\text{FET}}$  and the on/off ratio of the former (Supplementary Figure S9) were estimated to be  $1.1\text{ cm}^2\text{ V}^{-1}\text{ s}^{-1}$  and  $10^5$ , respectively. The transistor composed of C8-BTBT exhibited a high  $\mu_{\text{FET}}$  value of  $9.2\text{ cm}^2\text{ V}^{-1}\text{ s}^{-1}$  and an on/off ratio of  $10^9$  in the saturated regime, as displayed in Figure 4b and c, while the transistor composed of spin-coated C8-BTBT only exhibited a  $\mu_{\text{FET}}$  value of  $0.2\text{ cm}^2\text{ V}^{-1}\text{ s}^{-1}$  and an on/off ratio of  $10^4$ . The significantly enhanced electrical property in the former is primarily due to the optimized crystal alignment, as indicated by the XRD patterns and optical microscopy images. In addition, the growth direction of crystalline films is the same as that of the channel, which may yield a straightforward pathway for charge carriers. Also, the crystal islands separated by the Cytop guide layer are responsible for the reduced crosstalk effect, and thereby enhance the on-off ratio.

To further improve the device performance, we utilized the induced homogenous dewetting process to deposit doping layers at the interfaces of Au electrodes and organic semiconductors. The formation of charge injection layers of transition metal oxides (TMOs), such as molybdenum oxide ( $\text{MoO}_3$ ), vanadium oxide ( $\text{V}_2\text{O}_5$ ) and tungsten oxide ( $\text{WO}_3$ ), contributed to decreasing the charge injection barrier at the contact interface.<sup>36</sup> The transistor electrodes doped by TMOs can markedly increase the  $\mu_{\text{FET}}$  and lower the threshold voltage.<sup>37–39</sup> It was also reported that aqueous TMO solutions can be used for the doping process in solution-processed devices.<sup>40,41</sup> As shown in Figure 5a and Supplementary Figure S10, the hydrophilic source/drain electrodes on the hydrophobic substrate, combined with the Cytop guide layer, efficiently guide the spontaneous location of aqueous dopant solutions for the precise deposition of dopants. The real-time observation of the evolution of the water droplet in the bank region clearly illustrated that the TMOs finally only remained on the electrodes (Figure 5b). At the beginning, a  $0.1\text{-}\mu\text{L}$  droplet of  $\text{MoO}_3$  solution self-assembled into the electrode and channel area and then gradually shrunk as water evaporated. After 63 s, the droplet completely separated into two parts and then rapidly dried onto the electrodes. The whole process took approximately 70 s in total.

Figure 5c illustrates the doped device configuration, which exhibits an ultra-thin doping layer at the electrode/semiconductor interface in an OTFT device. Though the thickness of the doping layer could not be directly determined in our experiment, since the AuNPs have large sizes (10–30 nm), the doping effect could be determined by examining the enhancement of the device performance through electrical measurements. The transfer and output characteristics of a transistor doped by  $\text{MoO}_3$  are displayed in Figure 5d and e. This transistor exhibited a higher  $\mu_{\text{FET}}$  of  $13.1\text{ cm}^2\text{ V}^{-1}\text{ s}^{-1}$ , a smaller threshold voltage of 2.5 V compared with those of an undoped transistor. Moreover, the turn-on characteristics in Figure 5d became much sharper than those of the undoped transistor and exhibited a quite small threshold slope of 0.3 V/decade

To clarify the generality of the doping method, we prepared transistor arrays doped by  $\text{V}_2\text{O}_5$  or  $\text{WO}_3$ , characterized their charge carrier transport properties, and found that the average  $\mu_{\text{FET}}$  values were obviously increased after doping (Figure 5f) compared with those of an undoped transistor. The electric parameters of various devices are shown in Table 1. After TMO-doping through the homogenous

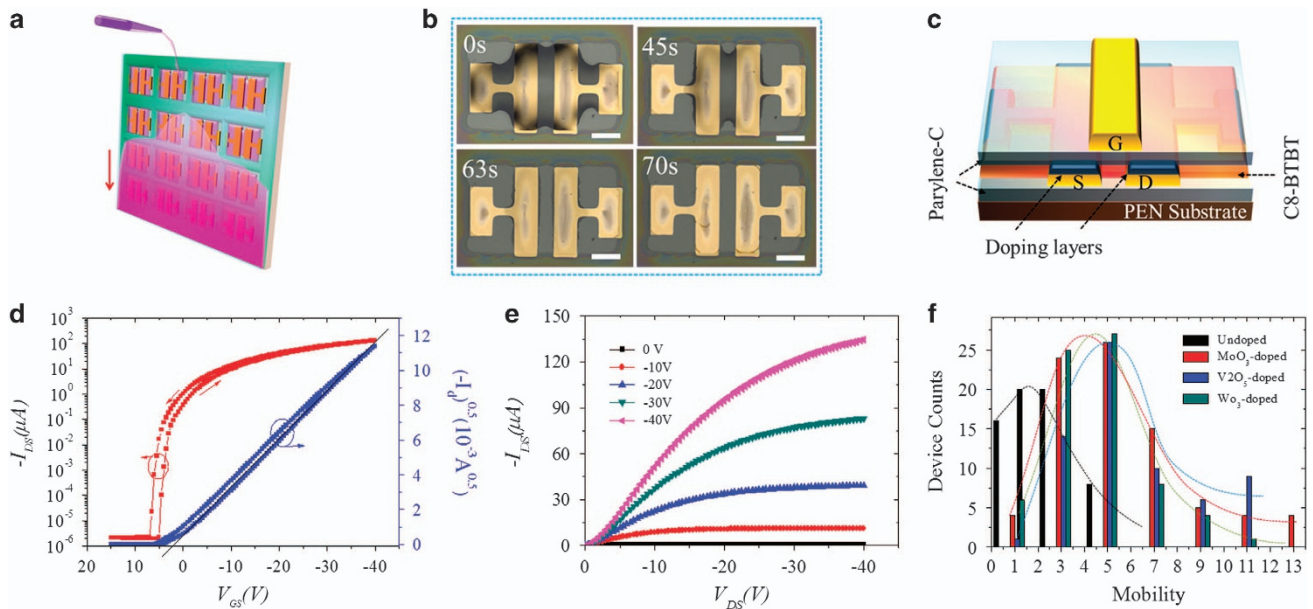


**Figure 5** (a) Illustration of the process for injecting aqueous TMO inks into the bank region. The microdroplets of aqueous TMO solutions were spontaneously injected into the banks due to the hydrophilic Au electrode surfaces. (b) Real-time observation of the drying dynamics of deposited aqueous TMO inks in the bank regions. The scale bars are 200  $\mu\text{m}$ . (c) Doped device configuration. (d, e) The transfer and output characteristics of the  $\text{MoO}_3$ -doped devices, respectively. The applied drain voltage was  $-40\text{ V}$ . (f) The mobility distribution in the undoped and doped devices.

**Table 1** Electrical parameters of the undoped and doped devices fabricated through the homogeneous dewetting method

Dopants	Maximum sat. mobility ( $\text{cm}^2\text{V}^{-1}\text{s}^{-1}$ )	Average sat. mobility ( $\text{cm}^2\text{V}^{-1}\text{s}^{-1}$ )	Threshold voltage (V)	Subthreshold slope		Contact resistance ( $k\ \Omega\text{cm}$ ) <sup>a</sup>
				(V/dec)	Log ( $I_{\text{on}}/I_{\text{off}}$ )	
Non	9.2	$3.4 \pm 1.7$	$3.4 \pm 1.6$	$0.45 \pm 0.21$	$8.78 \pm 0.43$	14.9
$\text{MoO}_3$	13.1	$5.5 \pm 2.8$	$1.7 \pm 0.7$	$0.35 \pm 0.13$	$8.05 \pm 0.35$	3.8
$\text{V}_2\text{O}_5$	11.6	$6.1 \pm 2.5$	$2.0 \pm 1.1$	$0.90 \pm 0.47$	$7.92 \pm 0.28$	7.7
$\text{WO}_3$	10.0	$4.4 \pm 1.9$	$0.7 \pm 0.2$	$0.56 \pm 0.28$	$7.85 \pm 0.33$	13.2

<sup>a</sup>The width-normalized contact resistances were extracted in the linear regimes at  $V_{\text{GS}}$  of  $-40\text{ V}$ .

dewetting method, the transistors exhibited much improved properties compared with the undoped transistor. In particular, it can be seen that the highest mobility appeared in the  $\text{MoO}_3$ -doped transistor, which exhibited a low threshold voltage and a small subthreshold slope, closely corresponding to the well-oriented crystalline film and the small contact resistance of 3.8  $k\Omega\text{ cm}$ . In addition, it is evident that  $\text{V}_2\text{O}_5$  and  $\text{WO}_3$  could also effectively enhance the transistor performance. As previously reported,  $\text{V}_2\text{O}_5$  and  $\text{WO}_3$  have a work function of 4.8 eV, while the value is 5.4 eV for  $\text{MoO}_3$ .<sup>37</sup> Hence, the latter is much more ideal as a charge carrier transfer layer between AuNPs and C8-BTBT. Based on these results, we clarified the feasibility of this new doping technique in fully printed flexible organic electronics. We also noted that parameters such as the average mobility and threshold voltage still had wide distribution, which could be overcome through further confinement of crystal growth.

## CONCLUSION

In summary, we developed a homogeneous dewetting technique on large-area MDAs by gravity-assisted deformation in droplets on a tilted substrate. It was found that increasing the tilt angle enabled the deformation of droplets, thus leading to the homogeneous receding of upper contact lines from top to bottom on the MDAs. Moreover, this method allows the deposition of discrete organic

semiconducting thin films for fully printed organic thin-film transistors. The obtained transistors exhibited a high mobility and on/off ratio of  $9.2\text{ cm}^2\text{ V}^{-1}\text{ s}^{-1}$  and  $10^9$ , respectively. Furthermore, we developed a solution process for *p*-type dopants in aqueous TMO solutions, which can be precisely deposited onto the bottom electrodes to tune the interfacial state, significantly enhancing the device performance. A smaller contact resistance of 3.8  $k\Omega\text{ cm}$  and a higher mobility of  $13.1\text{ cm}^2\text{ V}^{-1}\text{ s}^{-1}$  were realized. The current procedure enables fully solution-processed TFTs and the doping of electrodes, which are promising for high-resolution integrated electronic devices.

## CONFLICT OF INTEREST

The authors declare no conflict of interest.

## ACKNOWLEDGEMENTS

This work was financially supported by a Grant-In-Aid for Scientific Research (No. 26286040, 15K21617 and 17H02769) from the Ministry of Education, Culture, Sport, Science, and Technology of Japan; a Grant for Advanced Industrial Technology Development (No. 11B11016d) from the New Energy and Industrial Technology Development Organization (NEDO), Japan; the Henan Province Nature Science Fund (No. 162300410261) and Distinguished Youth Developed Science Fund (No. F0001182); the Guangdong Provincial Department of Science and Technology (Grant 2015B090924001); and in part by the Guangdong Natural Science Funds for Distinguished Young Scholars

(Grant 2016A030306046). We extend our thanks to Nippon Kayaku Co. and Dr. Takimiya (RIKEN) for providing us with C8-BTBT.

**Author contributions:** XL and CL performed the device design and fabrication and equally contributed to this work. KS, TY, JL, TY and PX contributed to the analysis of the deposited organic thin films. XL, CL and TM performed data analysis and manuscript preparation. MK prepared and provided the AuNP inks. JT helped with the data analysis and interpretation. TM supervised this project.

- Theberge, A. B., Courtois, F., Schaerli, Y., Fischlechner, M., Abell, C., Hollfelder, F. & Huck, W. T. Microdroplets in microfluidics: an evolving platform for discoveries in chemistry and biology. *Angew. Chem. Int. Ed.* **49**, 5846–5868 (2010).
- Leung, K., Zahn, H., Leaver, T. M., Konwar, K., Hanson, N. W., Pagé, A. P., Lo, C., Chain, P., Hallam, S. & Hansen, C. L. A programmable droplet-based microfluidic device applied to multiparameter analysis of single microbes and microbial communities. *Proc. Natl Acad. Sci.* **109**, 7665–7670 (2012).
- Wen, L., Tian, Y. & Jiang, L. Bioinspired Super-Wettability from Fundamental Research to Practical Applications. *Angew. Chem. Int. Ed.* **54**, 3387–3399 (2015).
- Wang, S., Liu, K., Yao, X. & Jiang, L. Bioinspired surfaces with superwettability: new insight on theory, design, and applications. *Chem. Rev.* **115**, 8230–8293 (2015).
- Lv, J., Song, Y., Jiang, L. & Wang, J. Bio-inspired strategies for anti-icing. *ACS nano* **8**, 3152–3169 (2014).
- Ueda, E. & Levkin, P. A. Emerging Applications of Superhydrophilic-Superhydrophobic Micropatterns. *Adv. Mater.* **25**, 1234–1247 (2013).
- Lai, Y., Pan, F., Xu, C., Fuchs, H. & Chi, L. *In Situ* Surface-Modification-Induced Superhydrophobic Patterns with Reversible Wettability and Adhesion. *Adv. Mater.* **25**, 1682–1686 (2013).
- Bai, H., Du, C., Zhang, A. & Li, L. Breath figure arrays: unconventional fabrications, functionalizations, and applications. *Angew. Chem. Int. Ed.* **52**, 12240–12255 (2013).
- Wang, J. Z., Zheng, Z. H., Li, H. W., Huck, W. T. S. & Siringhaus, H. Dewetting of conducting polymer inkjet droplets on patterned surfaces. *Nat. Mater.* **3**, 171–176 (2004).
- Li, Y., Ji, D., Liu, J., Yao, Y., Fu, X., Zhu, W., Xu, C., Dong, H., Li, J. & Hu, W. Quick fabrication of large-area organic semiconductor single crystal arrays with a rapid annealing self-solution-shearing method. *Sci. Rep.* **5**, 13195 (2015).
- Gundlach, D. J., Royer, J. E., Park, S. K., Subramanian, S., Jurchescu, O. D., Hamadani, B. H., Moad, A. J., Kline, R. J., Teague, L. C., Kirillov, O., Richter, C. A., Kushmerick, J. G., Richter, L. J., Parkin, S. R., Jackson, T. N. & Anthony, J. E. Contact-induced crystallinity for high-performance soluble acene-based transistors and circuits. *Nat. Mater.* **7**, 216–221 (2008).
- Pierre, A., Sadeghi, M., Payne, M. M., Facchetti, A., Anthony, J. E. & Arias, A. C. All-Printed Flexible Organic Transistors Enabled by Surface Tension-Guided Blade Coating. *Adv. Mater.* **26**, 5722–5727 (2014).
- Naab, B. D., Himmelberger, S., Diao, Y., Vandewal, K., Wei, P., Lussem, B., Salleo, A. & Bao, Z. High Mobility N-Type Transistors Based on Solution-Sheared Doped 6, 13-Bis (triisopropylsilyl)ethynyl pentacene Thin Films. *Adv. Mater.* **25**, 4663–4667 (2013).
- Diao, Y., Shaw, L., Bao, Z. & Mannsfeld, S. C. Morphology control strategies for solution-processed organic semiconductor thin film. *Energy Environ. Sci.* **7**, 2145–2159 (2014).
- Giri, G., Park, S., Vosguerichian, M., Shulaker, M. M. & Bao, Z. High-Mobility, Aligned Crystalline Domains of TIPS-Pentacene with Metastable Polymorphs Through Lateral Confinement of Crystal Growth. *Adv. Mater.* **26**, 487–493 (2014).
- Diao, Y., Tee, B. C., Giri, G., Xu, J., Kim, D. H., Beceril, H. A., Stoltenberg, R. M., Lee, T. H., Xue, G., Mannsfeld, S. C. & Bao, Z. Solution coating of large-area organic semiconductor thin films with aligned single-crystalline domains. *Nat. Mater.* **12**, 665–671 (2013).
- Wu, Y., Feng, J., Su, B. & Jiang, L. 3D Dewetting for Crystal Patterning: Toward Regular Single-Crystalline Belt Arrays and Their Functionality. *Adv. Mater.* **28**, 2266–2273 (2016).
- Minari, T., Kanehara, Y., Liu, C., Sakamoto, K., Yasuda, T., Yaguchi, A., Tsukada, S., Kashizaki, K. & Kanehara, M. Room-Temperature Printing of Organic Thin-Film Transistors with  $\pi$ -Junction Gold Nanoparticles. *Adv. Funct. Mater.* **24**, 4886–4892 (2014).
- Liu, X., Kanehara, M., Liu, C., Sakamoto, K., Yasuda, T., Takeya, J. & Minari, T. Spontaneous Patterning of High-Resolution Electronics via Parallel Vacuum Ultraviolet. *Adv. Mater.* **28**, 6568–6573 (2012).
- Tan, C. P. & Craighead, H. G. Surface engineering and patterning using parylene for biological applications. *Materials* **3**, 1803–1832 (2010).
- Kumatani, A., Liu, C., Li, Y., Darmawan, P., Takimiya, K., Minari, T. & Tsukagoshi, K. Solution-processed, self-organized organic single crystal arrays with controlled crystal orientation. *Sci. Rep.* **2**, 393–398 (2012).
- Lee, C. S., Lee, S. H., Park, S. S., Kim, Y. K. & Kim, B. G. Protein patterning on silicon-based surface using background hydrophobic thin film. *Biosens. Bioelectron.* **18**, 437–444 (2003).
- Jiang, H., Zhang, Y., Han, D., Xia, H., Feng, J., Chen, Q., Hong, Z. & Sun, H. Bioinspired Fabrication of Superhydrophobic Graphene Films by Two-Beam Laser Interference. *Adv. Funct. Mater.* **24**, 4595–4602 (2014).
- Neto, A. I., Correia, C. R., Custódio, C. A. & Mano, J. F. Biomimetic Miniaturized Platform Able to Sustain Arrays of Liquid Droplets for High-Throughput Combinatorial Tests. *Adv. Funct. Mater.* **24**, 5096–5103 (2014).
- Bowen, J. J., Taylor, J. M., Jurich, C. P. & Morin, S. A. Stretchable Chemical Patterns for the Assembly and Manipulation of Arrays of Microdroplets with Lensing and Micromixing Functionality. *Adv. Funct. Mater.* **25**, 5520–5528 (2015).
- Krasovitski, B. & Marmur, A. Drops down the hill: theoretical study of limiting contact angles and the hysteresis range on a tilted plate. *Langmuir* **21**, 3881–3885 (2005).
- Öner, D. & McCarthy, T. J. Ultrahydrophobic surfaces. Effects of topography length scales on wettability. *Langmuir* **16**, 7777–7782 (2000).
- Musterd, M., van Steijn, V., Kleijn, C. R. & Kreutzer, M. T. Droplets on inclined plates: Local and global hysteresis of pinned capillary surfaces. *Phys. Rev. Lett.* **113**, 066104 (2014).
- Le Grand, N., Daerr, A. & Limat, L. Shape and motion of drops sliding down an inclined plane. *J. Fluid Mech.* **541**, 293–315 (2005).
- Kimura, M., Misner, M. J., Xu, T., Kim, S. H. & Russell, T. P. Long-range ordering of diblock copolymers induced by droplet pinning. *Langmuir* **19**, 9910–9913 (2003).
- Quérel, D., Azzopardi, M. J. & Delattre, L. Drops at rest on a tilted plane. *Langmuir* **14**, 2213–2216 (1998).
- Santos, M. J., Velasco, S. & White, J. A. Simulation analysis of contact angles and retention forces of liquid drops on inclined surfaces. *Langmuir* **28**, 11819–11826 (2012).
- Furmidge, C. G. L. Studies at phase interfaces. I. The sliding of liquid drops on solid surfaces and a theory for spray retention. *J. Colloid Sci.* **17**, 309–324 (1962).
- Liu, C., Minari, T., Lu, X., Kumatani, A., Takimiya, K. & Tsukagoshi, K. Solution-Processable Organic Single Crystals with Bandlike Transport in Field-Effect Transistors. *Adv. Mater.* **23**, 523–526 (2011).
- Holzwarth, U. & Gibson, N. The Scherrer equation versus the 'Debye-Scherrer equation'. *Nat. Nanotech* **6**, 534–534 (2011).
- Meyer, J., Hamwi, S., Kröger, M., Kowalsky, W., Riedl, T. & Kahn, A. Transition metal oxides for organic electronics: energetics, device physics and applications. *Adv. Mater.* **24**, 5408–5427 (2012).
- Chu, C. W., Li, S. H., Chen, C. W., Shrotriya, V. & Yang, Y. High-performance organic thin-film transistors with metal oxide/metal bilayer electrode. *Appl. Phys. Lett.* **87**, 193508 (2005).
- Kumaki, D., Umeda, T. & Tokito, S. Reducing the contact resistance of bottom-contact pentacene thin-film transistors by employing a MoOx carrier injection layer. *Appl. Phys. Lett.* **92**, 13301 (2008).
- Kano, M., Minari, T. & Tsukagoshi, K. Improvement of subthreshold current transport by contact interface modification in p-type organic field-effect transistors. *Appl. Phys. Lett.* **94**, 143304 (2009).
- Kumaki, D., Fujisaki, Y. & Tokito, S. Reduced contact resistance and highly stable operation in polymer thin-film transistor with aqueous MoOx solution contact treatment. *Org. Electron.* **14**, 475–478 (2013).
- Shiwaku, R., Yoshimura, Y., Takeda, Y., Fukuda, K., Kumaki, D. & Tokito, S. Control of threshold voltage in organic thin-film transistors by modifying gate electrode surface with MoOx aqueous solution and inverter circuit applications. *Appl. Phys. Lett.* **106**, 053301 (2015).



This work is licensed under a Creative Commons Attribution 4.0 International License. The images or other third party material in this article are included in the article's Creative Commons license, unless indicated otherwise in the credit line; if the material is not included under the Creative Commons license, users will need to obtain permission from the license holder to reproduce the material. To view a copy of this license, visit <http://creativecommons.org/licenses/by/4.0/>

© The Author(s) 2017

Supplementary Information accompanies the paper on the NPG Asia Materials website (<http://www.nature.com/am>)